Canadian Science Publishing
NRC Research Press journals | Publishing Services

Canadian Journal of Chemistry
Revue canadienne de chimie

XEOL spectroscopy of lanthanides in aqueous solution

Journal:	*Canadian Journal of Chemistry*
Manuscript ID	cjc-2017-0038.R1
Manuscript Type:	Article
Date Submitted by the Author:	19-May-2017
Complete List of Authors:	Jürgensen, Astrid; Leibniz-Institut fur Analytische Wissenschaften - ISAS eV, Interface Processes
Is the invited manuscript for consideration in a Special Issue?:	TK Sham
Keyword:	XEOL spectroscopy, lanthanide ions, aqueous solutions, luminescence, rare earth elements Sm, Dy, and Tb

XEOL spectroscopy of lanthanides in aqueous solution

Astrid Jürgensen[1,2] *

[1] *Canadian Synchrotron Radiation Facility, Synchrotron Radiation Center, Stoughton WI, USA*

[2] *Leibniz-Institut für Analytische Wissenschaften – ISAS – e.V.*

Bunsen-Kirchhoff-Straße 11, 44139 Dortmund, Germany

* *tel.: +49 (0)231 1392-294, fax: +49 (0)231 1392-120, e-mail: astrid.juergensen@isas.de*

Abstract

As part of an ongoing study of the electronic interactions between solute and solvent molecules a method for X-ray Excited Optical Luminescence (XEOL) analysis of aqueous solutions was developed at the double-crystal-monochromator beamline (DCM) of the Canadian Synchrotron Radiation Facility (CSRF). It was tested using a series of solutions containing lanthanide ions. The samples were contained in a sample holder for liquids with a 3 μm Mylar window separating them from the vacuum ($\leq 3\times10^{-6}$ torr) in the solid state absorption chamber of the DCM beamline.

Terbium, samarium and dysprosium have four intense and narrow luminescence peaks between 450 and 700 nm, well separated from the luminescence peak of the Mylar window between 300 and 425 nm. The intensity of the rare earth (RE^{3+}) luminescence peaks was lower for the solutions than for solid $RECl_3 \cdot 6H_2O$. In part, this was caused by the lower RE^{3+} concentration in the solutions than in the solid. In addition, the solvent (water) acts as a quencher. The disorder and the molecular motion in the solution increase the availability of non-radiative de-excitation pathways. A high concentration of SO_4^{2-} in the solution enhanced the luminescence intensity, probably by inhibiting some non-radiative de-excitation pathways. This study has shown that it is in principle possible to investigate the luminescence of aqueous solutions with XEOL spectroscopy. Furthermore, it is possible to use this technique as a quantitative analytical tool for concentrated luminescent solutions and to study the shielding effects of anions in the solution that increase the luminescence intensity.

Keywords: XEOL spectroscopy; lanthanide ions; aqueous solutions; luminescence; rare earth elements Sm, Dy, and Tb

Introduction:

X-ray Excited Optical Luminescence (XEOL) Spectroscopy probes specific de-excitation mechanisms of a system following the absorption of an x-ray photon, namely those involving the emission of an optical photon.[1] It is used to study the origins of luminescence in materials,[1-5] and it can be applied as a probe to monitor radiation damage during protein x-ray crystallography studies[6] and pH-triggered drug release from nanoparticles.[7] The use of tunable x-rays from a synchrotron source allows the injection of photons at specific energies, e.g. near the absorption edge of an element leading to preferred core-excitation of that element. Thus, the technique is element specific. For example, it can be used to determine which chemical elements, in particular impurity elements, are involved in producing the luminescence, and how certain impurities might affect both emission wavelength and decay rate of the excited state.[8] In addition, x-ray absorption energies depend on the chemical environment of the absorbing atom, making it possible to study the correlation between luminescence and chemical environment of the absorbing atom of the same element.[9] The XEOL technique is also excitation channel specific. For example, the luminescence yield following C(1s) excitation of organic molecules or organic-ligand metal complexes depends on whether the core electron was excited to the π^* or the σ^* orbital.[10,11] This can provide information about the electronic structure of the valence shell and the chemical bonding in the sample. Recent developments in the technique include time resolution in the picosecond range[12,13] and the collection of 2D XAFS-XEOL spectra.[14]

In solids the x-ray absorption process creates holes in the valence shell and electrons in the conduction band either by direct absorption or indirectly following Auger or fluorescence decay of core-hole excited states. The drop of an electron from the conduction band into a valence band hole can lead to the emission of a photon (band-gap or band-edge luminescence). The wavelength of the emitted photon depends on the band-gap energy and the process is usually rapid due to the

short lifetime of the excited state (a few nanoseconds). Defects in the crystal structure or the presence of impurity atoms can lead to the formation of energy levels within the band-gap. Electrons from the conduction band can tunnel into these levels and then drop back into the valence band. The emitted photon has a longer wavelength than the band-gap luminescence and generally a longer decay rate, due to the longer lifetime of the excited state. Hence, there is a correlation between the luminescence and the crystallinity and the electronic structure of the sample. In particular, it provides information about the local electronic structure around the excited atom.

Similarly, in aqueous solutions the x-ray excitation leads to the formation of ions and molecules with valence shell holes, electrons in molecular antibonding orbitals and hydrated photoelectrons. Again, these species could have been created by direct photoabsorption or as products of core-hole de-excitation processes, e.g. Auger, fluorescence or fragmentation. Emission of a visible photon could result from the drop of an electron from an antibonding orbital into the valence shell, from the capture of a hydrated electron or from electron-transfer-reactions between various solvent and solute species. The last two processes often involve two or more steps. An XEOL study of ions in aqueous solution could thus provide information on the local structure of the solvent molecules around the solute ion, i.e. the hydration shell, on the electronic transitions between solute and solvent or between two different solute species, and on the specific mechanisms of these electron-transfer-reactions.

One group of luminescent ions in aqueous solution are the lanthanides. With the exception of La^{3+}([Xe]$4f^0$) and Lu^{3+}([Xe]$4f^{14}$) the lanthanide cations have partially filled 4f orbitals. Electronic de-excitation of a 4f excited state can lead to the emission of light which, depending on the lanthanide ion, ranges from the near IR (Nd^{3+}, Er^{3+} and Yb^{3+}),[15] through the visible (e.g. Tb^{3+}, Eu^{3+}, Dy^{3+} and Sm^{3+})[16] to the near uv (some Gd^{3+} complexes, e.g. $Gd^{3+}_{(aq)}$).[17,18] The luminescence

originates from parity forbidden transitions within the 4f orbital shell. The 4f orbitals are relatively deep inside the atom, i.e. localized. Hence, they are atomic in character. They interact only weakly with ligand orbitals and generally do not participate in chemical bonding. In consequence, the 4f excited states have long radiative lifetimes (0.1 – 1.0 ms) and very narrow emission bands.[19-21] Intensity and radiative lifetime depend upon the energy difference between the excited and the ground state of the ion and the availability of other competing non-radiative processes such as, internal conversion, intersystem crossing and cross-relaxation between neighbouring complexes. The greatest intensity and longest lifetime are observed for Gd^{3+}, followed by Tb^{3+} and Eu^{3+}.[22] In aqueous solution, however, the lanthanide luminescence is effectively quenched by water molecules,[22-24] and there have been numerous studies to find ligand molecules that shield the lanthanide ion from the water molecules and enhance the luminescence intensity relative to the aquo complex.[15,16,21,23,25-28] This interest originates from the fact that the lanthanide ions can be effective luminescent sensors and probes,[19,29] e.g., for temperature measurements[30] and for the detection of ions, organic molecules, water, and other species.[31-35] They can aid in the characterization of the structure of biological macromolecules such as proteins, nucleotides, nucleic acids and viruses,[23,36-39] and they are also useful for various bio-medical applications in drug development, genomic screening and clinical diagnostics.[16,20,27,30,40-46]

The present paper describes a methodology for soft x-ray (1800 – 4200 eV) XEOL measurements of aqueous solutions. It involves the use of a liquid cell[47] to isolate the solution from the vacuum of the sample chamber. Using aqueous solutions of $TbCl_3$, $DyCl_3$ and $SmCl_3$ as examples, this technique is investigated and discussed.

Experiment:

$DyCl_3 \cdot 6H_2O$, $SmCl_3 \cdot 6H_2O$ and $TbCl_3 \cdot 6H_2O$ powders (≥ 99% purity) were purchased from Sigma-Aldrich and used without further purification. A solid sample was prepared by crushing the powder with a mortar and pestle and then spreading a thin layer (~0.15 μm) onto a piece of double-sided carbon tape that was attached to a steel disk. This sample disk was then attached to a sample holder with the aid of double-sided carbon tape. ~1.0 mol/L solutions were prepared by dissolving appropriate amount of the powder in deionized water (5.00 ml for $DyCl_3$ and $SmCl_3$ and 2.00 ml for $TbCl_3$). Solutions with lower $[Tb^{3+}]$ for a concentration dependence study were prepared in the following way: An ~0.5 M $TbCl_3$ solution was prepared by dissolving the appropriate amount of solid in 10.00 ml of deionized water. Then 1.00 ml aliquots of this solution were diluted to 2.00 ml and 4.00 ml with deionized water to prepare ~0.25 M and ~0.125 M solutions, respectively. A summary of the solutions and their concentrations is given in Table 1. An aliquot (0.6 ml) of each solution was put into the sample holder for liquids that was designed for use at the double-crystal-monochromator beamline (DCM) of the Canadian Synchrotron Radiation Facility (CSRF).[47] A 3 μm Mylar window isolated the sample in the holder from the vacuum (~3×10^{-6} torr) in the solid-state absorption chamber.

The XEOL spectra were collected at the DCM beamline of CSRF which was located at the Synchrotron Radiation Center (SRC) of the University of Wisconsin, Madison in Stoughton, WI USA. Energy calibration of the incident x-ray photons was achieved by measurement of the XANES spectra of standards (powders of SiO_2, $Na_4P_2O_7$, $ZnSO_4$, KCl and $CaCO_3$) and then adjusting the energy scale using a 4th order polynomial function obtained from these standard spectra. The optical luminescence of the samples was recorded using a Jobin-Yvon 100 Spex H10/1200@450 spectrometer with a Hamamatsu R943 photomultiplier tube and C2761 detection unit. The incident photon beam was at a 45º angle to the sample surface, and the optical

spectrometer was mounted on a port of the vacuum chamber situated at a 90º angle to the incoming x-ray beam (Fig. 1). The wavelength scale was calibrated by measuring the XEOL spectrum of Cu-doped ZnS (commercial P-31 phosphor powder from USR Optonix Inc.) and setting the main peak of this spectrum to 530 nm. The total-electron-yield (TEY) signal from a gas cell containing ~1.3 torr air and located upstream from the sample was used to normalize the intensity of the XEOL spectra with respect to the incident photon flux.

A set of at least 4 scans was collected for each XEOL spectrum, using an incident x-ray energy of 2115 eV. Spikes caused by electrical noise were removed manually. Each scan was then normalized with respect to the incident photon flux by first subtracting the dark background signal, and then dividing by the TEY signal from the gas cell. The normalized data from the scans was averaged (Fig. 2a). Then the XEOL peak of the window was removed (Fig. 2b). For this, a least-squares fit was done on the spectral region between 200 and 450 nm using two XEOL spectra of water. The fit result is then subtracted from the spectrum of the solution to obtain the spectrum of the ion without the contribution from the window. Two water spectra are needed for the fit in order to account for changes in the XEOL of the window due to radiation damage. Finally, corrections for the variation in uv-visible light transmission of the window are made by dividing the measured XEOL spectrum of the aqueous ion by the uv-visible transmission of the 3 μm Mylar window material (Fig. 2c), determined experimentally with an Ocean Optics USB2000-UV-VIS spectrometer. The spectrum of an incandescent lamp was measured with and without the window between the light source and the detector, and the former spectrum was then divided by the latter to obtain the window transmission shown in Fig. 2c.

Results and Discussion

As discussed in detail previously,[47] the XANES analysis of aqueous solutions with soft x-

rays (~1800 to ~4000 eV) requires storage of the sample in a container that isolates it from the vacuum, while exposing it to the x-rays. This is accomplished with the aid of a thin-film window in the container. The material for this window has to withstand the pressure differential between the solution inside and the vacuum outside. It should be transparent to the x-rays, and it should also be robust, i.e. damage caused by the radiation should be minimal or, better yet, non-existent. For XEOL experiments the cell window must also be transparent to optical photons, and it should not luminesce in the visible region of the spectrum. Water is a very good quenching agent of optical luminescence,[22-24] and thus maximizing the incoming x-ray photon flux and the transmission by the window of both x-rays and optical photons is essential. Hence, a 3 μm Mylar window was used, and the experimental spectra were collected with the ring energy at 1 GeV and a photon energy of 2115 eV. This window material is transparent to visible light with a transmission of 70% – 90% over the entire range up to the cut-off point at ~330 nm (3.75 eV) in the near uv (Fig. 2c). Unfortunately, the window material, a polycarbonate, luminesces. The XEOL spectrum has a peak at 365 nm (3.40 eV) (Fig. 2b, centre). Furthermore, the shape of the XEOL peak changes with prolonged x-ray exposure (Fig. 2b, centre) caused by the gradual deterioration of the Mylar by the x-rays (radiation damage). Thus, with the present experimental setup XEOL spectroscopy of aqueous solutions is limited to systems which emit optical photons with wavelengths greater than ~450 nm, as is the case for the rare-earth ions Dy^{3+}, Sm^{3+} and Tb^{3+}.

Of the three rare-earth elements studied, Tb^{3+} has the most intense luminescence (Fig. 3a, Table 2) with four intense and narrow peaks between 450 and 650 nm, well separated from the luminescence peak of the Mylar window. These four peaks result from the $^5D_4 \rightarrow {}^7F_{6,5,4,3}$ transitions (Table 2). There are also peaks at longer ($^5D_4 \rightarrow {}^7F_{2,1}$ transitions) wavelengths with much lower intensity. An energy level schematic for these transitions is shown in Fig. 4. The

intensity of the four main peaks decreases by a factor of ~50 for the 0.913 M Tb^{3+} solution, compared to solid state $TbCl_3 \cdot 6H_2O$ (Fig. 3b, Table 2). Although [Tb^{3+}] in the solution (5.5×10^{20} atoms/cm^3) is only ~8% of the value in the solid (7×10^{21} atoms/cm^3), the actual number of Tb^{3+} ions probed in the solution (8.82×10^{15}) is ~50% of that probed in the solid (1.67×10^{16}) due to the larger attenuation length in the solution (6.972 μm) than in the solid (1.036 μm). Thus, the lower number of ions in the sample should only account for a factor of 2 in the luminescence intensity reduction.

The additional quenching is caused by the greater number of H_2O molecules in the first coordination shell and by the greater disorder in the solution compared to the solid. The main non-radiative de-excitation of Tb^{3+} is via vibronic coupling of the $^5D_4$ excited state to the O-H oscillators in the first coordination shell,[36] as shown in Fig. 4. The coordination number of Tb is 8 in solid $TbCl_3 \cdot 6H_2O$, all six H_2O molecules and two Cl^- ions are part of the first coordination shell: $(Tb(H_2O)_6Cl_2)^+$. The Tb^{3+} aquo complex in solution has 9 H_2O molecules in the first coordination shell: $(Tb(H_2O)_9)^{3+}$.[36] There is thus an addition to the first coordination shell, changing its size and shape, and there is also a change in its composition: two Cl^- ions are replaced by three H_2O molecules. This increases the rate constant for the radiationless de-excitation pathway, thus decreasing the luminescence intensity. The greater mobility of the ions and water molecules in the solution might cause an additional increase in the radiationless de-excitation rate.

The relative intensities of the peaks also change in solution compared to the solid. In particular, there is a 10% intensity increase of peaks #1 and #3 relative to peak #2. This might also be caused by the change in the local chemical environment – i.e. the first coordination shell – of the Tb^{3+} ion, see above (peaks #1 and #3 are sensitive to the chemical environment[38]). Alternatively, this could be caused by a difference in the transmission of optical photons between

the solid and the solution, or it could be an artifact of the background removal mechanism. Further experiments are needed in order to clarify this.

The intensity of the luminescence from solid state $DyCl_3 \cdot 6H_2O$ (Fig. 5a) is about a factor of 30 less compared to that from solid state $TbCl_3 \cdot 6H_2O$ (Fig. 3a). The four observable peaks result from $^4F_{9/2} \rightarrow {}^6H_{x/2}$ transitions (Table 2). The two most intense of these Dy^{3+} peaks occur in the same wavelength region as those of Tb^{3+}, and these two are the only ones observed in the XEOL spectrum of an ~0.9 M aqueous $DyCl_3$ solution (Fig. 5b). Due to the intensity decrease caused by the decreased Dy^{3+} concentration and the H_2O quenching, the two peaks are barely resolved from the background (Fig. 5b). The loss in intensity for the solution relative to the solid is of comparable magnitude for Dy^{3+} as for Tb^{3+}, a factor of ~50. There also appears to be a change of the relative peak intensities (Fig. 5, Table 2), but given the overall low intensity of the solution spectrum, this might be an artifact of the background removal.

The luminescence intensity of Sm^{3+} from solid state $SmCl_3 \cdot 6H_2O$ is even less (Fig. 6a) – about $^1/_{10}{}^{th}$ that of solid $DyCl_3 \cdot 6H_2O$ and about $^1/_{400}{}^{th}$ that of solid $TbCl_3 \cdot 6H_2O$ – and the peak positions are shifted toward the red by 50 – 85 nm compared to the main peaks of Tb^{3+} (Table 2). The peaks result from $^4G_{5/2} \rightarrow {}^6H_{x/2}$ transitions. No luminescence was detected for a 0.913 M aqueous solution of $SmCl_3$. This is not unexpected: an intensity reduction by a factor of ~50, as observed for Tb^{3+} and Dy^{3+}, would reduce the height of the most intense Sm^{3+} peak to 9 counts, well below the detection limit of the spectrometer.

The dependence of the signal intensity on the ion concentration was tested for Tb^{3+} by measurement of the XEOL spectra of solutions with different ion concentrations, listed in Table 1. The XEOL spectra obtained for these solutions show that measurement is possible for Tb^{3+} concentrations as low as 0.120 M (Fig. 7a). The intensity of the signal increases with increasing ion concentration. For all four luminescence peaks the increase in peak height with respect to ion

concentration is not linear, as can been seen from Fig. 7b. The formula for the luminescence intensity I_L,

(1) $$I_L(\lambda_{ex}) = \Phi_L\, I_0(\lambda_{ex}) \left(1 - 10^{-\varepsilon_L(\lambda_{ex}) b C_L}\right)$$

with Φ_L = luminescence quantum yield, $I_0(\lambda_{ex})$ = incident light intensity, $\varepsilon_L(\lambda_{ex})$ = molar absorptivity, λ_{ex} = wavelength of the incident light, b = path length, and C_L = solute concentration,[48] significantly overestimated the peak height at the lowest concentration (0.120 M) for all four peaks. However, adding a constant intensity loss term I_c (equation (2)) resulted in a good fit to the experimental data over the entire concentration range investigated (Fig. 7b).

(2) $$I_L(\lambda_{ex}) = \Phi_L\, I_0(\lambda_{ex}) \left(1 - 10^{-\varepsilon_L(\lambda_{ex}) b C_L} - I_C\right)$$

Equation (1) is based on the assumption that the incident light is either transmitted or absorbed by the solution, and the additional term I_c required to fit the experimental data suggests the presence of another material which absorbs a constant amount of the incident light independent of $[Tb^{3+}]$. A possible candidate for this is the Mylar window that according to theoretical calculations[49] absorbs ~14% of the incident radiation I_0 at 2115 eV, in reasonable agreement with the average value of 0.20 ± 0.02 (20% of I_0) determined for I_c (Fig. 7b, Table 3). However, other factors, e.g. scattering of the incident radiation by the solution, probably also contribute to I_c. Extrapolation of the best fit curves down to zero intensity gives a detection limit of $[Tb^{3+}]$ ~ 0.08 mol/L.

It is possible to reduce the quenching effect of the H_2O molecules by using rare-earth complex ions, where the coordinated ligands exclude water from the first coordination sphere,[36, 37] or act as an antenna enhancing the luminescence.[27,40] Even the presence of some anions in high concentration can enhance the intensity of the observed luminescence.[50] With the present experimental setup it was possible to detect the luminescence of a 0.0121 M $TbCl_3$ solution containing 3.99 M $(NH_4)_2SO_4$ (Fig. 8). Initial results from molecular dynamics calculations

(Supplementary Material) suggest that SO_4^{2-} anions replace some of the H_2O molecules in the first hydration shell, thereby reducing the quenching of the luminescence.

Conclusions

This study has shown that it is in principle possible to investigate the luminescence of aqueous solutions with incident radiation in the soft x-ray region (1800 – 4200 eV). Furthermore, it is possible to use XEOL spectroscopy as a quantitative analytical tool for concentrated Tb^{3+} solutions, and to study the shielding effects of anions in the solution that increase the luminescence intensity. Combining XEOL spectroscopy with x-ray photoabsorption could aid in the study of ligand-ion interactions and electron-transfer-reactions in aqueous solution. The recent addition of timing capabilities to the optical spectrometer[12,13,51,52] will also allow the determination of decay rates of the luminescence, providing additional information about the systems being studied. However, the experimental setup imposes some restrictions on the types of system to be studied. Of the lanthanides only Tb and perhaps Eu emit visible light in the correct wavelength range ($\lambda > 450$ nm) and at sufficiently high intensity to make the study of aqueous solutions with concentrations much less than 1.0 M feasible. Similarly, other luminescent species, e.g. $Ru(bipyridyl)_3^{2+}$, various nanoparticles or other luminophores in solution, can only be investigated, if the emitted light has a wavelength greater than 450 nm and an intensity comparable to that of $Tb^{3+}(aq)$.

Supplementary Material

Information on the molecular dynamics calculations of aqueous $TbCl_3$ and $TbCl_3$ + $(NH_4)_2SO_4$ solutions is provided online.

Acknowledgements

The experimental work was conducted at the Canadian Synchrotron Radiation Facility (CSRF) which was funded by NSERC – CRSNG (Natural Sciences and Engineering Research Council of Canada – Conseil de recherches en sciences naturelles et en génie du Canada) and NRC – CRNC (National Research Council Canada – Conseil national de recherches du Canada). It was located at the Synchrotron Radiation Center (SRC) of the University of Wisconsin-Madison. Funding for this facility was provided by NSF (Award No.: DMR-00537588). The author also thanks Dan Wallace for providing the Ocean Optics USB2000-UV-VIS spectrometer of SRC to measure the uv-vis transmission of the 3 µm Mylar film. The Leibniz Institut für Analytische Wissenschaften – ISAS – e.V. is funded by the Ministerium für Innovationen, Wissenschaft und Forschung des Landes Nordrhein-Westfalien, Germany and by the Bundesministerium für Bildung und Forschung, Germany.

References:

(1) Sham, T. K. *J. Electron Spectrosc.* **2015**, 204, 196. doi: 10.1016/j.elspec..04.004

(2) Peng M.; Li Y.; Gao J.; Zhang D.; Jiang Z.; Sun X. *J. Phys. Chem. C* **2011**, 115, 11420. doi: 10.1021/jp201884y

(3) Paik T.; Gordon T. R.; Prantner A. M.; Yun H.; Murray C. B. *ACS Nano* **2013**, 7, 2850. doi: 10.1021/nn4004583

(4) Ward M. J.; Rupar P. A.; Murphy M. W.; Yiu Y.-M.; Baines K. M.; Sham T.K. *J. Phys. Conf. Ser.* **2013**, 430, 012046. doi: 10.1088/1742-6596/430/1/012046

(5) Zhang D.; Zhang H.; Zhang X.; Sham T.-K.; Hu Y.; Sun X. *Phys. Chem. Chem. Phys.*

2016, 18, 6406. doi: 10.1039/c5cp05764g

(6) Owen R. L.; Yorke B. A.; Pearson A. R. *Acta Crystallogr. D* **2012** 68, 505. doi: 10.1107/S0907444912002946

(7) Chen H.; Moore T.; Qi B.; Colvin D. C.; Jelen E. K.; Hitchcock D. A.; He J.; Mefford O. T.; Gore J. C.; Alexis F.; Anker J. N. *ACS Nano* **2013**, 7, 1178. doi: 10.1021/nn304369m

(8) Soderholm, L.; Liu, G. K.; Antonio, M. R.; Lytle, F. W. J. Chem. Phys. **1998**, 109, 6745. doi: 10.1063/1.477320

(9) Sham, T.; Jiang, D.; Coulthard, I.; Lorimer, J.; Feng, X.; Tan, K.; Frigo, S.; Rosenberg, R.; Houghton, D.; Bryskiewicz, B. *Nature* **1993**, 363, 331. doi:10.1038/363331a0

(10) Naftel, S.; Kim, P.-S. G.; Sham, T.; Sammynaiken, R.; Yates, B.; Hu, Y.-F. *J. Appl. Phys.* **2003**, 93, 5191. doi: 10.1063/1.1565492

(11) Naftel, S.; Zhang, P.; Kim, P.-S.; Sham, T.; Coulthard, I.; Antel Jr. W.; Freeland, J.; Frigo, S.; Fung, M.-K.; Lee, S.; Hu, Y.; Yates, B. *Appl. Phys. Lett.* **2001**, 78, 1847. doi: 10.1063/1.1358360

(12) Ward M. J.; Regier T. Z.; Vogt J. M.; Gordon R. A.; Han W.-Q.; Sham T. K. *J. Phys. Conf. Ser.* **2013**, 425, 092006. doi: 10.1088/1742-6596/425/9/092006

(13) Mosselmans J. F. W.; Taylor R. P.; Quinn P. D.; Finch A. A.; Cibin G.; Gianolio D.; Sapelkin A. V. *J. Phys. Conf. Ser.* **2013**, 425, 182009. doi: 10.1088/1742-6596/425/18/182009

(14) Ward M. J.; Smith J. G.; Regier T. Z.; Sham T. K. *J. Phys. Conf. Ser.* **2013**, 425, 132009. doi: 10.1088/1742-6596/425/13/132009

(15) Klink, S. I.; Hebbink, G. A.; Grave, L.; Peters, F. G. A.; van Veggel, F. C. J. M.; Reinhoudt, D. N.; Hofstraat, J. W. Eur. *J. Org. Chem.* **2000**, 1923. doi: 10.1002/(SICI)1099-0690(200005)2000:10<1923::AID-EJOC1923>3.0.CO;2-W

(16) Petoud, S.; Cohen, S. M.; Bünzli, J.-C. G.; Raymond, K. N. *J. Am. Chem. Soc.* **2003**, 125, 13324. doi: 10.1021/ja0379363

(17) Lis, S.; Kimura, T.; Yoshida, Z. *J. Alloy Compd.* **2001**, 323-324, 125. doi: 10.1016/S0925-8388(01)00980-X

(18) Vuilleumier, J.-J.; Deschaux, M.; Marcantonatos, M. D. *J. Chem. Soc. Faraday T. 1* **1989**, 85, 2605. doi: 10.1039/F19898502605

(19) Parker, D. *Coord. Chem. Rev.* **2000**, 205, 109. doi: 10.1016/S0010-8545(00)00241-1

(20) Sabbatini, N.; Guardigli, M.; Lehn, J.-M. *Coord. Chem. Rev.* **1993**, 123, 201. doi: 10.1016/0010-8545(93)85056-A

(21) Choppin, G. R.; Peterman, D. R. *Coord. Chem. Rev.* **1998**, 174, 283. doi: http://dx.doi.org/10.1016/S0010-8545(98)00125-8

(22) Lis, S.; Kimura, T.; Yoshida, Z.; But, S. *J. Alloy Compd.* **2004**, 380, 173. doi: 10.1016/j.jallcom.2004.03.026

(23) Lis, S. *J. Alloy Compd.* **2002**, 341, 45. doi: 10.1016/S0925-8388(02)00055-5

(24) Beeby, A.; Clarkson, I. M.; Dickins, R. S.; Faulkner, S.; Parker, D.; Royle L.; de Sousa, A. S.; Williams, J. A. G.; Woods, M. *J. Chem. Soc. Perkin T. 2* **1999**, 3, 493. doi: 10.1039/A808692C

(25) Patroniak, V.; Baxter, P. N. W.; Lehn, J.-M.; Hnatejko, Z.; Kubicki, M. *Eur. J. Inorg.*

Chem. **2004**, 2379. doi: 10.1002/ejic.200300868

(26) Hebbink, G. A.; Reinhoudt, D. N.; van Veggel, F. C. J. M. *Eur. J. Org. Chem.* **2001**, 4101. doi: 10.1002/1099-0690(200111)2001:21<4101::AID-EJOC4101>3.0.CO;2-9

(27) Steemers, Frank, J.; Verboom, W.; Reinhoudt, D. N.; van der Tol, E. B.; Verhoeven, J. W. *J. Am. Chem. Soc.* **1995**, 117, 9408. doi: 10.1021/ja00142a004

(28) van Veggel, F. C. J. M.; Reinhoudt, D. N. *Chem.-Eur. J.* **1999**, 5, 90. doi: 10.1002/(SICI)1521-3765(19990104)5:1<90::AID-CHEM90>3.0.CO;2-8

(29) Richardson, F. S. *Chem. Rev.* **1982**, 82, 541. doi: 10.1021/cr00051a004

(30) Zhao, D.; Zhang, J.; Yue, D.; Lian, X.; Cui, Y.; Yang, Y.; Qian, G. *Chem. Commun. (Camb.)* **2016**, 52, 8259. doi: 10.1039/c6cc02471h

(31) de Bettencourt-Dias, A.; Barber, P. S.; Viswanathan, S. *Coord. Chem. Rev.* **2014**, 273-274, 165. doi: 10.1016/j.ccr.2014.04.010

(32) Yan, W.; Zhang, C.; Chen, S.; Han, L.; Zheng, H. *ACS Appl. Mater. Interfaces* **2017**, 9, 1629. doi: 10.1021/acsami.6b14563

(33) Sahoo, J.; Arunachalam, R.; Subramanian, P. S.; Suresh, E.; Valkonen, A.; Rissanen, K.; Albrecht, M. *Angew. Chem. Int. Ed. Engl.* **2016**, 55, 9625. doi: 10.1002/anie.201604093

(34) Dong, Y.; Cai, J.; Fang, Q.; You, X.; Chi, Y. *Anal. Chem.* **2016**, 88, 1748. doi: 10.1021/acs.analchem.5b03974

(35) Vanek, J.; Lubal, P.; Hermann, P.; Anzenbacher, P., Jr. *J. Fluoresc.* **2013**, 23, 57. doi: 10.1007/s10895-012-1116-3

(36) Horrocks, W. D., Jr.; Sudnick, D. R. *J. Am. Chem. Soc.* **1979**, 101, 334. doi:

10.1021/ja00496a010

(37) Horrocks, W. D., Jr.; Sudnick, D. R. *Accounts Chem. Res.* **1981**, 14, 384. doi: 10.1021/ar00072a004

(38) Cotton, S. A. Lanthanide and Actinide Chemistry, chapter 5 - *Electronic and Magnetic Properties of the Lanthanides*, pages 61 - 87. John Wiley & Sons, Ltd, Chichester, West Sussex, England UK, 2006.

(39) Penas, C.; Mascareñas, J. L.; Vázquez, M. E. *Chem. Sci.* **2016**, 7, 2674. doi: 10.1039/C5SC04501K

(40) Mathis, G. *Clin. Chem.* **1993**, 39, 1953. http://clinchem.aaccjnls.org/content/39/9/1953

(41) Soini, E. *Trends Anal. Chem.* **1990**, 9, 90. doi: 10.1016/0165-9936(90)87086-2

(42) DaCosta, M. V.; Doughan, S.; Han, Y.; Krull, U. J. *Anal. Chim. Acta* **2014**, 832, 1. doi: 10.1016/j.aca.2014.04.030

(43) Tu, D.; Zheng, W.; Liu, Y.; Zhu, H.; Chen, X. *Coord. Chem. Rev.* **2014**, 273-274, 13. doi: 10.1016/j.ccr.2013.11.017

(44) Liu, Q.; Feng, W.; Li, F. *Coord. Chem. Revi.* **2014**, 273-274, 100. doi: 10.1016/j.ccr.2014.01.004

(45) Surender, E. M.; Bradberry, S. J.; Bright, S. A.; McCoy, C. P.; Williams, D. C.; Gunnlaugsson, T. *J. Am. Chem. Soc.* **2017**, 139, 381. doi: 10.1021/jacs.6b11077

(46) Hao, J.-N.; Yan, B. *Adv. Funct. Mater.* **2016**, 1603856. doi: 10.1002/adfm.201603856

(47) Jürgensen, A. *Can. J. Chem.* **2009**, 87, 601. doi: 10.1139/V09-023

(48) Credi A.; Prodi L. *Spectrochim. Acta A* **1998**, 54, 159. doi: 10.1016/S1386-1425(97)00224-2

(49) Gullikson, E. (2010). Filter Transmission (X-ray transmission of a solid). *X-Ray Interactions With Matter.* Retrieved 17, January 2017, 2017, from http://henke.lbl.gov/optical_constants/filter2.html (http://henke.lbl.gov/optical_constants/)

(50) Kumala, S.; Hakanen, A.; Laine, E.; Haapakka, K. *J. Alloy Compd.* **1995**, 225, 279. doi: 10.1016/0925-8388(94)07141-1

(51) Heigl, F.; Jürgensen, A.; Zhou, X.-T.; Lam, S.; Murphy, M.; Ko, J. Y. P.; Sham, T. K.; Rosenberg, R. A.; Gordon, R.; Brewe, D.; Regier, T.; Armelao, L. *Dynamic view on nanostructures: a technique for time resolved optical luminescence using synchrotron light pulses at SRC, APS, and CLS*. In J.-Y. Choi and S. Rah, editors, Synchrotron Radiation Instrumentation: 9th International Conference on Synchrotron Radiation Instrumentation, volume 879 of AIP Conference Proceedings, pages 1202 - 1205, **2007**.

(52) Heigl, F.; Jürgensen, A.; Zhou, X.-T.; Murphy, M.; Ko, J. Y. P.; Lam, S.; Sham, T. K.; Regier, T.; Blyth, R. I. R.; Coulthard, I.; Zuin, L.; Hu, Y.-F.; Armelao, L., Gordon, R.; Brewe, D. *Time Resolved Studies of ZnO (Eu) Nanostructure Luminescence Using Short Synchrotron Radiation Pulses*. In B. Hedman and P. Pianetta, editors, X-RAY ABSORPTION FINE STRUCTURE - XAFS13: 13th International Conference, volume 882 of AIP Conference Proceedings, pages 864 - 866. **2007**.

Table 1: The aqueous solutions, their concentration and preparation method

rare-earth (RE) ion	*[RE^{3+}] mol/L*	*Preparation Method*
Dy^{3+}	~0.9[a]	1.9181 g $DyCl_3 \cdot 6H_2O$ dissolved in 5.00 ml deionized H_2O
Sm^{3+}	0.913	1.8474 g $SmCl_3 \cdot 6H_2O$ dissolved in 5.00 ml deionized H_2O
Tb^{3+}	0.913	0.7565 g $TbCl_3 \cdot 6H_2O$ dissolved in 2.00 ml deionized H_2O
	0.480	1.8881 g $TbCl_3 \cdot 6H_2O$ dissolved in 10.00 ml deionized H_2O
	0.240	1.00 ml of 0.480 M Tb^{3+} solution diluted to 2.00 ml
	0.120	1.00 ml of 0.480 M Tb^{3+} solution diluted to 4.00 ml
	0.0121	0.0227 g $TbCl_3 \cdot 6H_2O$ and 2.6383 g $(NH_4)_2SO_4$ dissolved in 5.00 ml deionized H_2O ($[SO_4^{2-}]$ = 3.99 M)

[a]The nominal concentration is 0.917 M Dy^{3+}. However, the solid sample contained an unknown impurity, which did not dissolve. Thus, the actual $[Dy^{3+}]$ is less than 0.917 M.

398 Table 2: Luminescence Peaks and their Assignment

Tb^{3+}	*solid $TbCl_3 \cdot 6H_2O$*		*0.913 M $TbCl_3$ solution*		
No.	*Position (nm)*	*Height (counts) [Rel. Height]*	*Position (nm)*	*Height (counts) [Rel. Height]*	*Assignment*
1	484	87953 [42.6]	482	1998 [53.0]	$^5D_4 \rightarrow {}^7F_6$
2	539	206074 [100]	537	3769 [100]	$^5D_4 \rightarrow {}^7F_5$
3	580	47115 [22.9]	578	1211 [32.1]	$^5D_4 \rightarrow {}^7F_4$
4	614	26487 [12.9]	613	591 [15.7]	$^5D_4 \rightarrow {}^7F_3$
5	642	3811 [1.85]	638	40 [1.06]	$^5D_4 \rightarrow {}^7F_2$
6	665	3879 [1.88]	665	65 [1.72]	$^5D_4 \rightarrow {}^7F_1$
Dy^{3+}	*solid $DyCl_3 \cdot 6H_2O$*		*~0.9 M $DyCl_3$ solution*		
No.	*Position (nm)*	*Height (counts) [Rel. Height]*	*Position (nm)*	*Height (counts) [Rel. Height]*	*Assignment*
1	475	5301 [85.1]	474	138 [100]	$^4F_{9/2} \rightarrow {}^6H_{15/2}$
2	568	6232 [100]	567	96 [69.6]	$^4F_{9/2} \rightarrow {}^6H_{13/2}$
3	655	297 [4.77]			$^4F_{9/2} \rightarrow {}^6H_{11/2}$
4	746	282 [4.53]			$^4F_{9/2} \rightarrow {}^6H_{9/2}$
Sm^{3+}	*solid $SmCl_3 \cdot 6H_2O$*		*0.913 M $SmCl_3$ solution*		

No.	*Position (nm)*	*Height (counts) [Rel. Height]*	*Position (nm)*	*Height (counts) [Rel. Height]*	*Assignment*
1	557	91 [20.4]			$^4G_{5/2} \rightarrow {}^6H_{9/2}$
2	593	447 [100]			$^4G_{5/2} \rightarrow {}^6H_{7/2}$
3	639	316 [70.7]			$^4G_{5/2} \rightarrow {}^6H_{5/2}$
4	697	63 [14.1]			$^4G_{5/2} \rightarrow {}^6H_{3/2}$

399

400 Table 3: The Intensity vs. [Tb^{3+}] correlation and the lowest detectable concentration

No.	Best Fit: *Peak Height* = $A\,(1-10^{-B\times[Tb^{3+}]}-C)$	[Tb^{3+}] for *Peak Height = 0*
1	A = 2790, B = 1.25, C = 0.21	0.082
2	A = 5192, B = 1.13, C = 0.18	0.078
3	A = 1670, B = 1.18, C = 0.19	0.079
4	A = 839, B = 1.24, C = 0.22	0.088
Average:	B = 1.20 ± 0.05, C = 0.20 ± 0.02	0.082 ± 0.004

401 **Note:** $A = k\, I_0(\lambda_{ex})\, \Phi_L$, $B = \varepsilon_L(\lambda_{ex})\, b$, and $C = I_c$. See text and equations (1) and (2) for details.

List of Figures:

Fig. 1. Setup of the experimental apparatus at the DCM beamline of CSRF.

Fig. 2. The extraction of the XEOL signal of the solute from the measured XEOL spectrum, illustrated for the data of a 0.480 M $TbCl_3$ solution:
a) top: the as collected data of a single scan
centre: the data of a single scan after despiking
bottom: the data of a single scan after background removal and I_0 normalization.
b) top: the averaged data of four scans (black) and the spectrum resulting from a least-squares fit (grey) on the 200 – 450 nm region using two XEOL spectra of water.
centre: the two XEOL spectra of water used for the least-squares fit.
bottom: The XEOL spectrum of the solute after subtraction of the contribution from the window and the water, the least-squares fit result.
c) bottom: the XEOL spectrum of the solute
top: the XEOL spectrum of the solute after normalization with respect to the transmission of the 3 μm Mylar window (grey).

Fig. 3. The XEOL spectrum of $TbCl_3$ in the solid state (a) and as a 0.913 M aqueous solution (b). For the latter, the spectrum prior to the subtraction of the window contribution is also shown (grey).

Fig. 4. The energy level diagram for the observed luminescent f-f transitions of Tb^{3+} and the radiationless de-excitation via O-H vibrations.

Fig. 5. The XEOL spectrum of $DyCl_3$ in the solid state (a) and as a ~0.9 M aqueous solution (b). For the latter, the spectrum prior to the subtraction of the window contribution is also

shown (grey).

Fig. 6. The XEOL spectrum of $SmCl_3$ in the solid state (a) and as a 0.913 M aqueous solution (b). For the latter, the spectrum prior to the subtraction of the window contribution is also shown (grey).

Fig. 7. The effect of ion concentration on the XEOL spectrum of Tb^{3+}(aq):

a) XEOL spectra of aqueous solutions with varying Tb^{3+} concentration showing the decrease in signal intensity.

b) The luminescence intensity (peak height) as a function of $[Tb^{3+}]$ for each of the four most intense peaks in the XEOL spectrum. The curves represent the best fits of the form $Peak\ Height = A\left(1 - 10^{-B[Tb^{3+}]}\right)$ (dotted grey) and $Peak\ Height = A\left(1 - 10^{-B[Tb^{3+}]} - C\right)$ (solid black), where $A = k\, I_0(\lambda_{ex})\, \Phi_L$, $B = \varepsilon_L(\lambda_{ex})\, b$, and $C = I_c$. See text and equations (1) and (2) for details.

Fig. 8. The XEOL spectrum of an aqueous solution containing 0.0121 M $TbCl_3$ and 3.99 M $(NH_4)_2SO_4$. The spectrum prior to the subtraction of the window contribution is shown in grey.

441 **Fig. 1.**

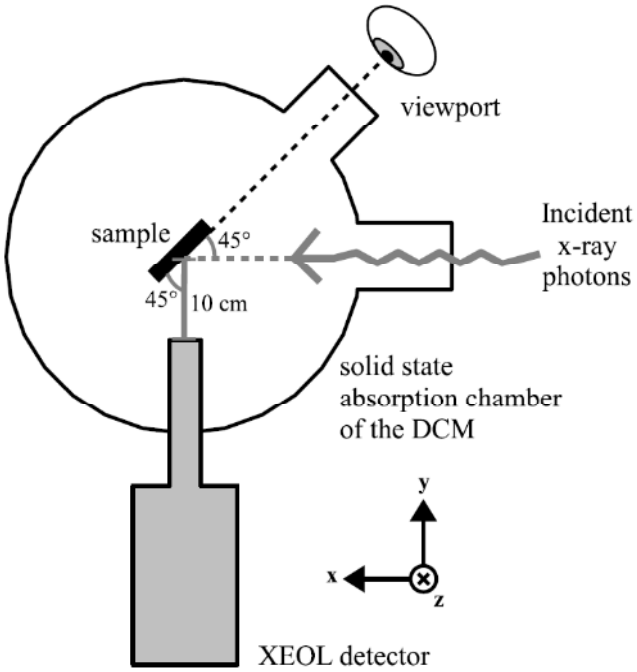

442

443

444 **Fig. 2.**

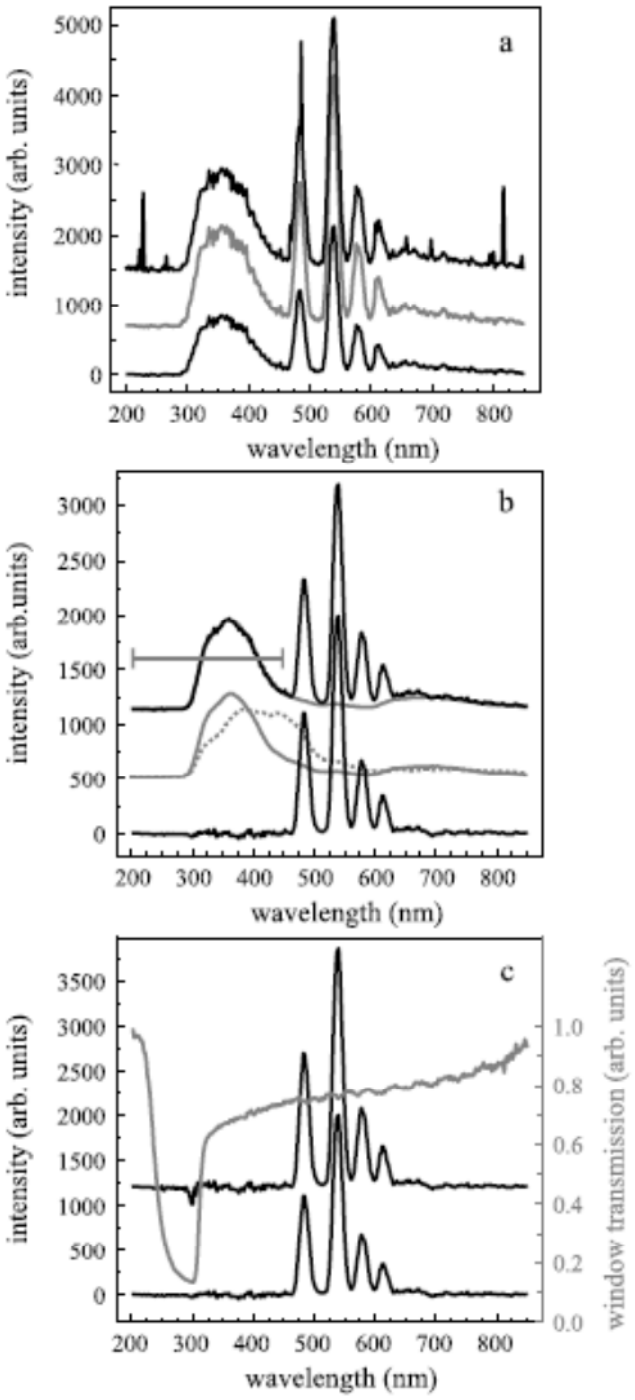

445

446

447 **Fig. 3.**

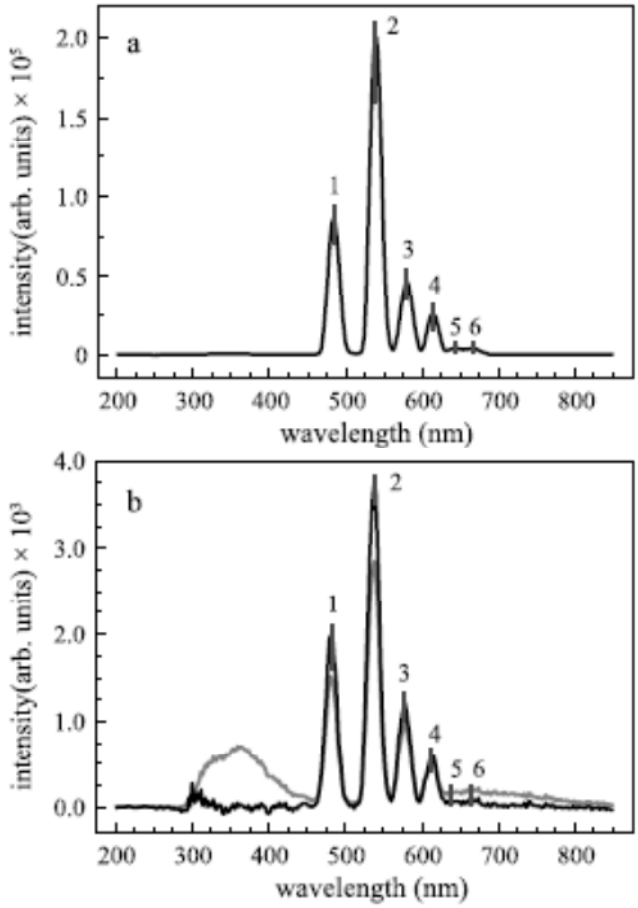

448

449

Fig. 4.

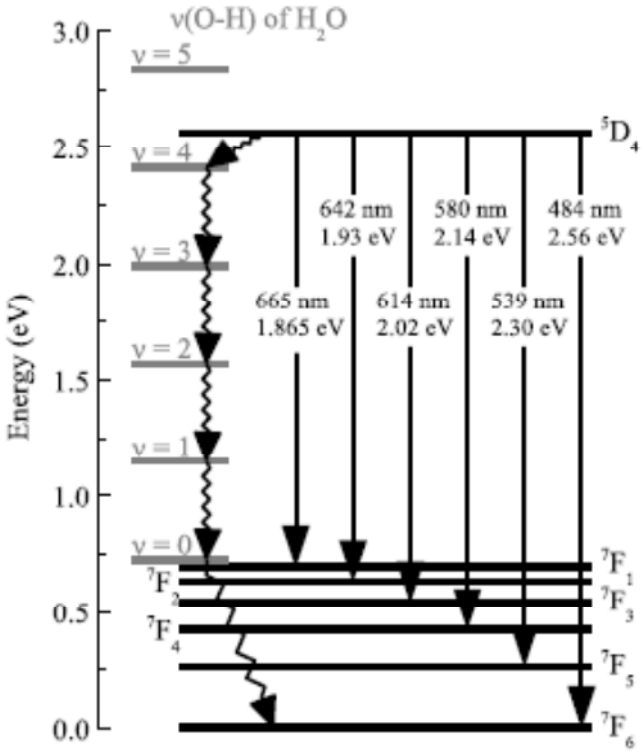
ν(O-H) of H2O
ν = 5
ν = 4
ν = 3
ν = 2
ν = 1
ν = 0
5D4
7F1
7F2
7F3
7F4
7F5
7F6
642 nm
1.93 eV
580 nm
2.14 eV
484 nm
2.56 eV
665 nm
1.865 eV
614 nm
2.02 eV
539 nm
2.30 eV
Energy (eV)
3.0
2.5
2.0
1.5
1.0
0.5
0.0

453 **Fig. 5.**

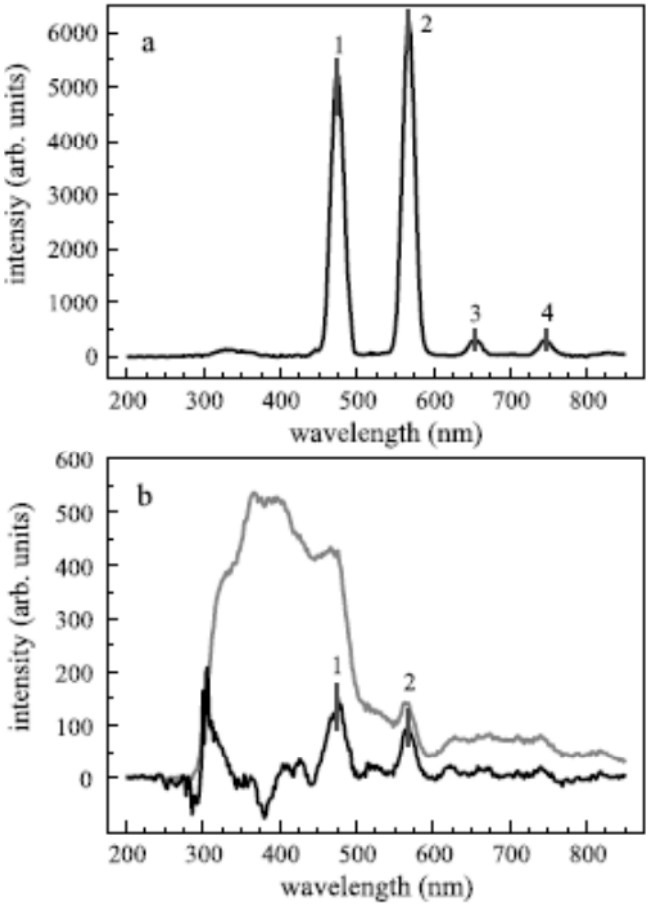

454

455

456 **Fig. 6.**

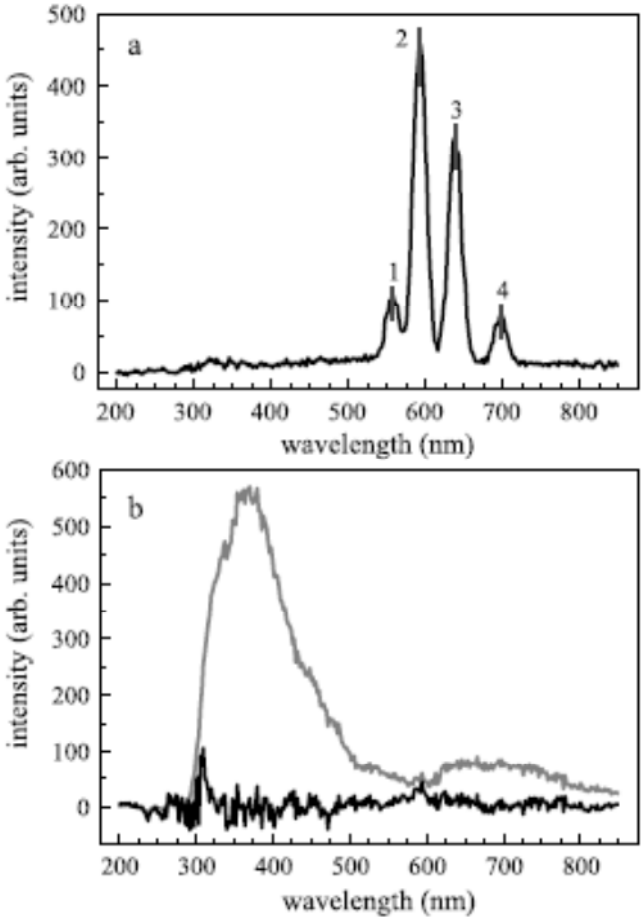

457

458

459 **Fig. 7.**

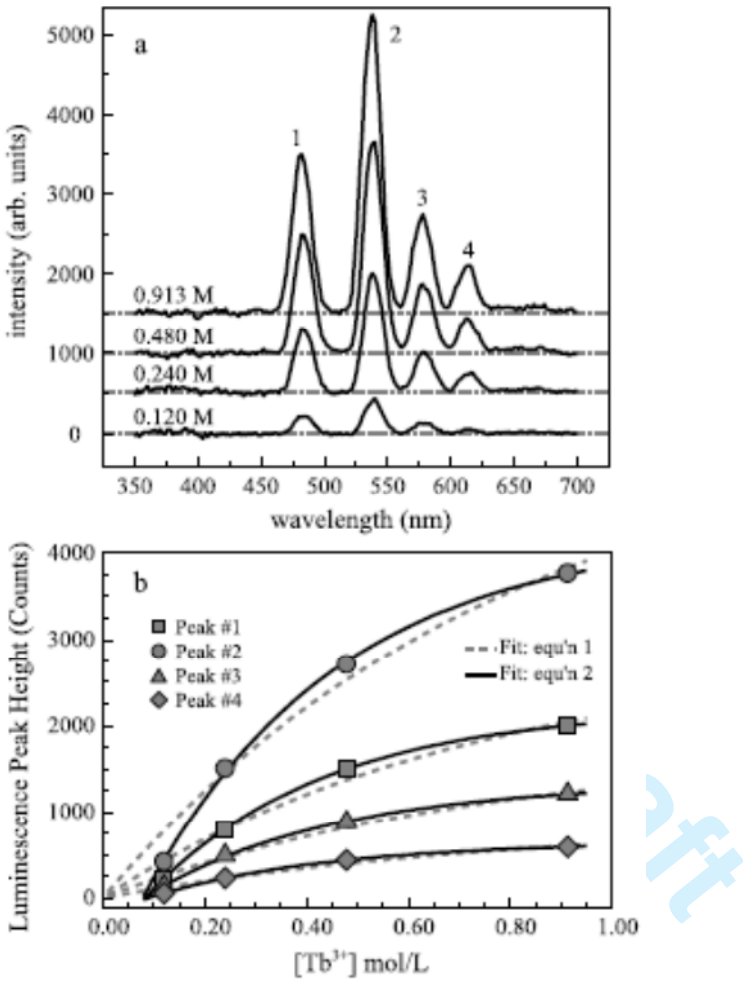

460

461

462 **Fig. 8.**

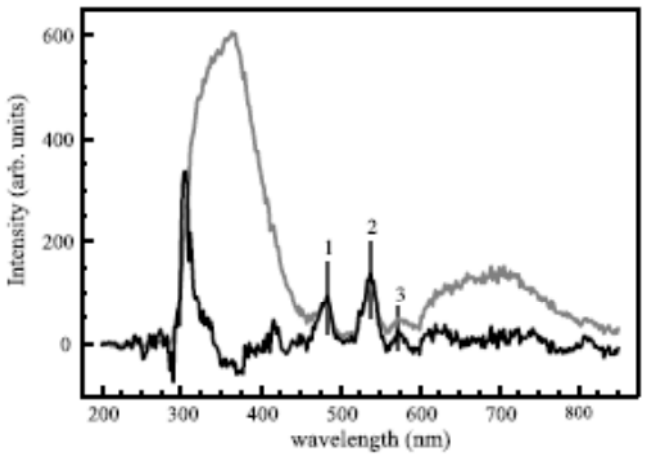

463

464

Graphical Abstract